



Structural Basis of Binding by Cyclic Nonphosphorylated Peptide Antagonists of Grb7 Implicated in Breast Cancer Progression

Nigus D. Ambaye¹†, Stephanie C. Pero²†, Menachem J. Gunzburg¹, MinYin Yap¹, Daniel J. Clayton¹, Mark P. Del Borgo¹, Patrick Perlmutter³, Marie-Isabel Aguilar¹, Girja S. Shukla², Elena Peletskaya², Michelle M. Cookson², David N. Krag², Matthew C. J. Wilce^{1*}‡ and Jacqueline A. Wilce^{1*}‡

¹Department of Biochemistry and Molecular Biology, Monash University, Wellington Road, VIC 3800, Australia

²Department of Surgery and Vermont Cancer Center, University of Vermont, Burlington, VT 05405, USA

³School of Chemistry, Monash University, Wellington Road, VIC 3800, Australia

Received 8 June 2011;
received in revised form
13 July 2011;
accepted 14 July 2011
Available online
23 July 2011

Edited by I. Wilson

Keywords:

Grb7 inhibitor;
SH2 domain;
cyclic peptide;
ITC;
phage display

Growth-receptor-bound protein (Grb)7 is an adapter protein aberrantly overexpressed, along with the erbB-2 receptor in breast cancer and in other cancers. Normally recruited to focal adhesions with a role in cell migration, it is associated with erbB-2 in cancer cells and is found to exacerbate cancer progression *via* stimulation of cell migration and proliferation. The G7-18NATE peptide (sequence: WFEgyDNTfPC cyclized *via* a thioether bond) is a nonphosphorylated peptide that was developed for the specific inhibition of Grb7 by blocking its SH2 domain. Cell-permeable versions of G7-18NATE are effective in the reduction of migration and proliferation in Grb7-overexpressing cells. It thus represents a promising starting point for the development of a therapeutic against Grb7. Here, we report the crystal structure of the G7-18NATE peptide in complex with the Grb7-SH2 domain, revealing the structural basis for its interaction. We also report further rounds of phage display that have identified G7-18NATE analogues with micromolar affinity for Grb7-SH2. These peptides retained amino acids F2, G4, and F9, as well as the YDN motif that the structural biology study showed to be the main residues in contact with the Grb7-SH2 domain. Isothermal titration calorimetry measurements reveal similar and better binding affinity of these peptides compared with G7-18NATE. Together, this study facilitates the optimization of second-generation inhibitors of Grb7.

© 2011 Elsevier Ltd. All rights reserved.

*Corresponding authors. E-mail addresses:
matthew.wilce@monash.edu; jackie.wilce@monash.edu.

† N.D.A. and S.C.P. are joint first authors.

‡ M.C.J.W. and J.A.W. are joint senior authors.

Abbreviations used: Grb, growth-receptor-bound protein; FAK, focal adhesion kinase; PDB, Protein Data Bank; ITC, isothermal titration calorimetry; HRP, horseradish peroxidase.

Introduction

Growth-receptor-bound protein (Grb)7 belongs to a family of adapter proteins that interact with upstream phosphorylated tyrosine kinases in the propagation of signal transduction pathways. Under normal cellular conditions, Grb7 plays a role in integrin-mediated cell migration *via* direct interaction with focal adhesion kinase (FAK) at focal

contacts (reviewed in Refs. 1 and 2). This is consistent with its evolutionary relationship to the Mig10 cell migration protein of *Caenorhabditis elegans*.³ Grb7 has become of particular interest, however, in cancer cells where it is massively overexpressed and interacts with the well-known propagator of cancerous cell growth, the erbB-2 (also known as Neu/HER-2/EGFR-2) receptor.⁴ Grb7 is tightly coamplified with erbB-2 in approximately 20–25% of breast cancer cell lines, and there is also a strong correlation between erbB-2 and Grb7 overexpression in esophageal, gastric, and ovarian cancers.^{5–7} Grb7 overexpression has been noted in 32% of Barrett's adenocarcinomas⁸ and has been correlated with poor prognosis for hepatocellular carcinoma.⁹ Most recently, a study of high Grb7 expression in 638 primary breast cancer specimens was found to correlate with decreased survival of the patients.¹⁰

There is now compelling evidence that the overexpression of Grb7 directly impacts the proliferative and metastatic potential of these cancers (and is not just a benign result of amplification that occurs due to the close proximity of the Grb7 gene to the erbB-2 gene on the 17q12 amplicon). In recent studies correlating Grb7 overexpression with clinical outcome, Grb7 protein overexpression has been shown to be an adverse prognostic factor in human breast cancer independent of erbB-2.^{10,11} In studies designed to directly determine the role of Grb7, it has been shown that the removal of Grb7 from breast cancer cells (using RNAi) reduces breast cancer cell viability and increases the activity of the anti-erbB-2 cancer therapeutic lapatinib.^{12,13} Grb7 overexpression in breast cancer cells has been shown to facilitate the phosphorylation of erbB-2 and AKT and, in mouse xenograft studies, promote the xenograft growth.¹⁴ It thus appears that Grb7 upregulation acts in concert with erbB-2 to promote cancer cell proliferation. With respect to its role in metastasis, overexpression of Grb7 has been shown to enhance cell migration, whereas inhibition of Grb7 (by overexpression of the Grb7 SH2 domain acting as a dominant-negative inhibitor) results in the inhibition of cell migration.^{15,16} More recently, knockdown of Grb7 expression in hepatocellular carcinoma cells resulted in their lower invasive potential *in vitro* and the delayed onset of tumors in nude mice.⁹ In another study, the knockdown of Grb7 using RNAi showed a strong antimigratory effect in a pancreatic cell line.¹⁷ Grb7 is thus now recognized to play a significant role in cancer progression and to be an important new therapeutic target.^{10,18}

Grb7 is a 532-residue protein composed of an N-terminal proline-rich domain, followed by an RA (Ras-associating) domain, a central PH (pleckstrin homology) domain, a BPS (between PH domain and SH2 domain) domain, and a C-terminal SH2

domain.^{2,19} It interacts with the phosphorylated tyrosine of activated upstream partners *via* its SH2 domain and is phosphorylated at specific tyrosine residues to propagate downstream events.^{20,21} While a large number of binding partners functioning upstream of Grb7 have been identified,²² the precise downstream events leading to cell proliferation and migration are not fully elucidated. The most recent data suggest that the proliferative activity of Grb7-overexpressing cells is mediated *via* the recruitment of RasGTPases and subsequent phosphorylation of extracellular signal-regulated kinase 1/extracellular signal-regulated kinase 2 leading to cell proliferation.²³ The way in which the Grb7/FAK interaction impacts migration in human cancer cells is not yet determined, but there is evidence to suggest that the phosphorylation of Grb7 by FAK impacts at the level of translational regulation.^{21,24}

The Grb7-SH2 domain has thus been targeted in the development of a specific peptide inhibitor of Grb7. The G7-18NATE peptide (sequence: WFE-GYDNTFPC cyclized *via* a thioether bond) was discovered using phage display and was found to be a specific inhibitor of Grb7, binding to the Grb7-SH2 domain with micromolar affinity, but it does not bind to the SH2 domains of Grb14 and Grb10, which are closely related family members, or to the Grb2-SH2 domain, which is the downstream partner of the erbB-2 receptor in normal cells.^{25–27} A cell-permeable version of G7-18NATE (synthesized with a Penetratin® or Tat-based C-terminal peptide extension) was shown to enhance the antiproliferative effect of Herceptin in breast cancer cells, successfully validating the principle of Grb7 inhibition through the blocking of its SH2 domain.²⁸ In another study, cell-permeable G7-18NATE was shown to prevent the Grb7 interaction with FAK and dramatically reduce cell migration in a pancreatic cell line.¹⁷ Together, these investigations demonstrate that G7-18NATE not only is a valuable tool for the inhibition of Grb7 in cells but also represents proof of concept that Grb7 may be blocked *via* its SH2 domain and that this may be to therapeutic advantage.

While G7-18NATE is effective as a Grb7 inhibitor, a pressing goal is to develop analogues with enhanced affinity. This would allow cellular experiments to be conducted at lower inhibitor concentrations and be an essential criterion for therapeutic use. What is not yet known is why the G7-18NATE peptide sequence has affinity and specificity for the Grb7-SH2 domain. Here, we report a breakthrough in the understanding of the structural basis for the G7-18NATE/Grb7-SH2 domain interaction through structural studies and through further peptide library screening. We report the crystal structure of G7-18NATE bound to the Grb7-SH2 domain, revealing the conformation adopted by

G7-18NATE and the critical contacts that underlie the basis for the interaction. We also report the outcome of further rounds of phage display that have provided second-generation peptides based upon G7-18NATE. These peptides are characterized and analyzed in light of the structural information for the further development of potent and specific Grb7 inhibitors.

Results

Structure of the G7-18NATE/Grb7-SH2 complex

In order to investigate the basis for the molecular interaction between the G7-18NATE peptide and the Grb7-SH2 domain, we solved the structure of the complex using X-ray crystallography to 2.4 Å resolution. The final G7-18NATE/Grb7-SH2 complex structure consists of four chains of the Grb7-SH2 domain and two G7-18NATE molecules in the asymmetric unit. This unexpected stoichiometry is most likely due to the crystal packing arrangement. The G7-18NATE binds at the expected site on the surface of the Grb7-SH2 molecule, but its presence occludes the binding site on an adjacent Grb7-SH2 domain. The Grb7-SH2 also formed dimers as previously observed.²⁶ The crystal is thus composed of Grb7-SH2 dimers in which one monomer of each dimer is peptide bound (chains A and B) and the other is apo-Grb7-SH2 (chains C and D).

The Grb7-SH2 domain adopts an SH2 domain fold, with an $\alpha\beta\alpha\beta\beta\beta\alpha$ configuration as seen also for its apo-form crystallized under different conditions²⁶ (Fig. 1a and b). Note that the standard nomenclature for SH2 domain secondary structures devised by Eck *et al.* is adopted throughout this report.²⁹ A three-stranded antiparallel β -sheet composed of β B, β C, and β D is flanked by the two helices α A and α B. The β D strand is extended and also forms a short region of β -sheet with β E. The intervening loops are named after their adjacent secondary structural elements. Short regions of β -sheet (β A, β F, and β G) observed in other SH2 domains are not present in the Grb7-SH2 domain, and an extra N-terminal helix is observed in this Grb7-SH2 construct, termed H1.

The G7-18NATE peptide is bound across the β D strand and makes contact with the BC, EF, and BG loops (Fig. 1c). The specific Grb7 amino acids that are involved in interactions are indicated with dots above the Grb7 sequence shown in Fig. 1a and further discussed below. The presence of G7-18NATE does not make significant impact on the structure of the protein, with the C $^{\alpha}$ RMSD between G7-18NATE-bound and apo-forms of the Grb7-SH2 domain being 0.54 Å for the cocrystallized Grb7-SH2 domain (across 96 atoms) and 0.71 Å for the

Grb7-SH2 domain structure previously reported [Protein Data Bank (PDB) ID: 2QMS] (across 99 atoms) (Fig. 1d).

G7-18NATE binding interactions with the Grb7-SH2 domain

The main objective of this study was to determine the structural basis for the G7-18NATE interaction with the Grb7-SH2 domain. For clarity, amino acid residues of G7-18NATE will be referred to using single-letter code, while those of the Grb7-SH2 domain will be referred to using three-letter code. The whole of the G7-18NATE peptide was clearly visible in the electron density map (Fig. 2a). The structure reveals the G7-18NATE arranged in a cycle with a pseudo- β -turn formed between the carbonyl of the N-terminal acetamide (to which the thioether is connected) and the amine of F9 (Fig. 2b). This turn is also stabilized by the trans conformation of P10 and the formation of a hydrogen bond between the backbone amine of C11 and the backbone carbonyl of F9. A β -turn is formed between F2 and Y5, with a hydrogen bond between the F2 carbonyl and the Y5 amine. No side-chain-specific intramolecular interactions appear to influence the conformation of the G7-18NATE. Rather, the side chains are arranged to either form contacts with the surface of the Grb7-SH2 domain, including hydrogen-bond, electrostatic, and van der Waals interactions, or extend into solvent.

The YDN residues of G7-18NATE that comprise the recognition motif of the Grb7-SH2 domain are positioned analogously to the pYXN mode of binding to the Grb2-SH2 domain,³⁰ which also possesses specificity for a YXN motif. Interestingly, this occurs despite the lack of a phosphate group (Fig. 2c). The tyrosine (Y5) side chain projects into the phosphotyrosine binding pocket with its aromatic ring positioned planar to the surface of the side chain of the critical Grb7 β D6 residue Leu481. The aspartic acid (D6) residue extends in the opposite direction and forms hydrogen bonds *via* its side-chain carbonyl and backbone amine with the Grb7 His479 backbone amine and carbonyl, respectively. Asparagine (N7) is extended back towards Leu481 where it forms bipartite hydrogen bonds with the backbone amide and carbonyl groups of Leu481. The G7-18NATE, as mentioned above, is nonphosphorylated. Grb7 residues that would be predicted to form electrostatic interactions with a phosphate include Arg438 and Arg458. In the current structure, the side chain of Arg438 extends to hydrogen bond with the carbonyl of glycine (G4).

Strikingly, the aromatic groups of the phenylalanines (F2 and F9) are positioned planar to the surface of the Grb7-SH2 domain contributing to binding *via* van der Waals contacts (Fig. 2d). F9 is positioned over the surface of the EF loop. In particular, this

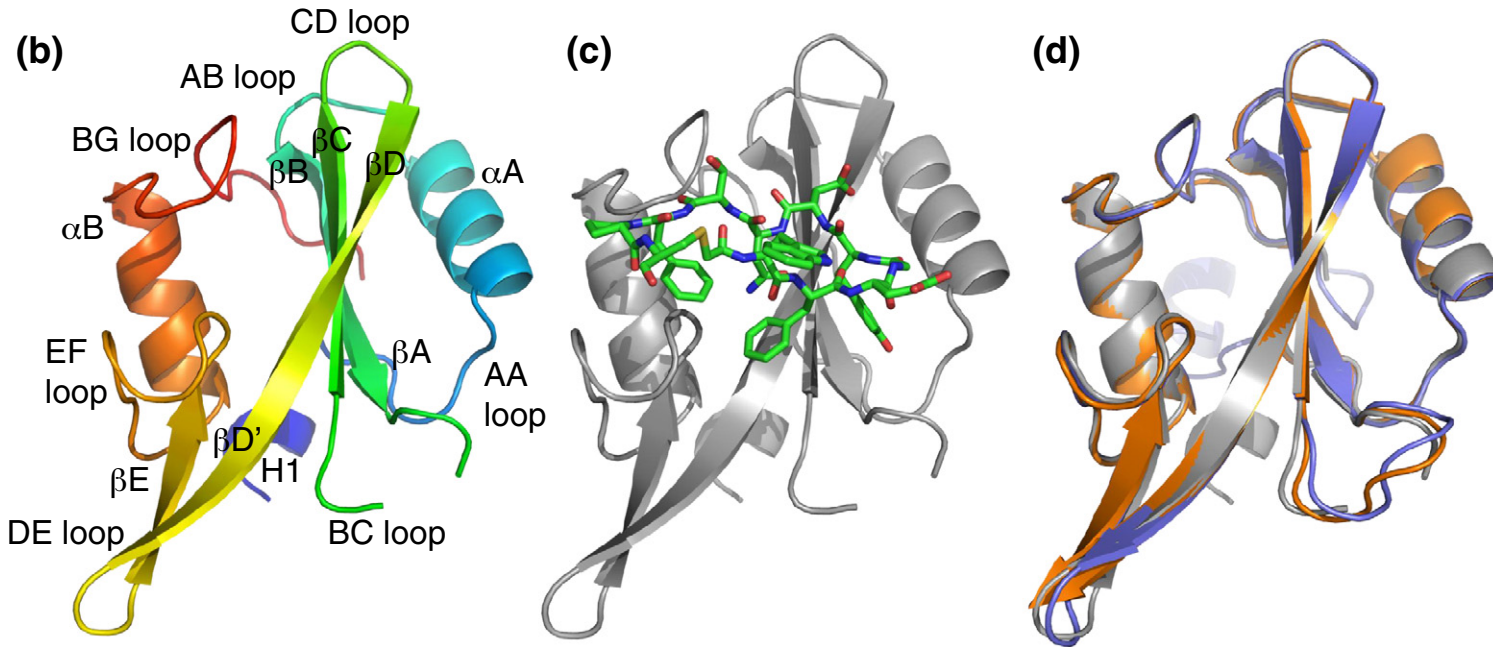
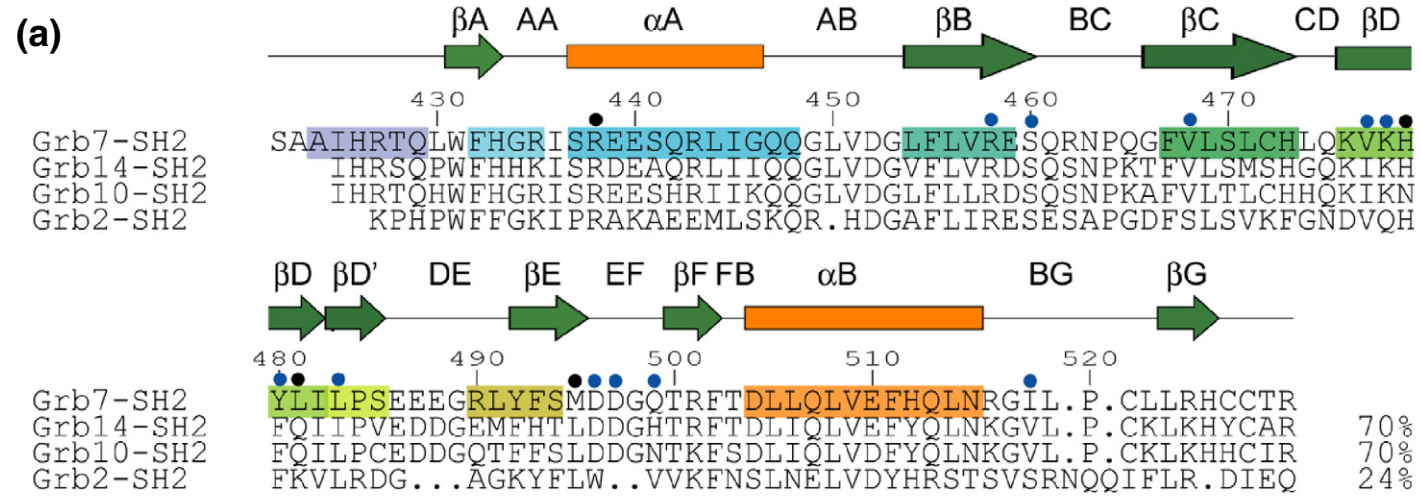


Fig. 1 (legend on next page)

surface is formed by the planar arrangement of the backbone carbons and C^β of Asp496. F2 is positioned over the surface of the Leu481 side chain adjacent to the surface that Y5 is positioned over. These residues contribute to a total surface area of interaction of 458 Å².

The remaining amino acid residues of G7-18NATE appear to play no role in forming interactions with the Grb7-SH2 domains at all. W1 projects away from the surface of interaction into solvent. Likewise, E3 projects away from the binding site, although in this case, it is not projecting into solvent. Rather, the E3 side chain forms hydrogen bonds with Arg458 in the phosphotyrosine binding site of an adjacent holo-Grb7-SH2 molecule. T8 also projects outward from the binding site, not forming any contacts with the Grb7-SH2 protein. The proline (P10) does not make any specific contribution to binding, although it may act to stabilize the turn conformation of the G7-18NATE. Lastly, cysteine appears to play no role in binding to the Grb7-SH2 domain except to provide the thiol for the cyclization of the peptide that is essential for binding.²⁵

Phage display evolution of second-generation peptides

In parallel with establishing the determinants of binding of G7-18NATE to the Grb7-SH2 domain using a structural method, we also sought to investigate the sequence requirements of the peptide using combinatorial peptide library screening. Affinity maturation of G7-18NATE was performed using a biased phage library approach with two additional rounds of library construction. The first-round libraries were designed with conserved YDN amino acids and the cyclic structure of Grb7 peptide retained using cysteines for disulfide bond cyclization. The YDN positions were identified from the original biased library screening where G7-18 was discovered.²⁵ Two libraries containing the YDN motif were created, one maintaining the four amino acids flanking each cysteine and the other with the flanking amino acids removed since it was not clear whether these amino acids were important for the binding. The cysteine-constrained libraries were designed with X₄CX₃YDNX₄CX₄ and CX₃YDNX₄C

(where X is any amino acid), referred to as the YDN and YDN-NA biased libraries, respectively. After three rounds of panning, we observed strong enrichment of 163-fold in the YDN-NA library and 12-fold in the YDN library. One hundred unique clones from the eluate collected from the YDN-NA library were screened for their binding to the SH2 domain of Grb7. There were 24 unique clones identified from 189 clones sequenced from the YDN and YDN-NA libraries. From this pool of unique clones, four clones (5073, 5200, 5242, and 5367) displayed improved binding to the SH2 domain of Grb7. Interestingly, the four strongest binding clones share a similar amino acid sequence with each other and with our original G7-18 clone (Table 1). The motif CX₁FX₂GYDNX₃(X₄=F/Y/W)(X₅=L/V)C was conserved in these peptides. This set of data showed that F at position 3 and G at position 5 are important. There was no preferential amino acid for the X₁ position; however, at the following positions, preference was shown for the following amino acids: X₂=W; X₃=E; X₄=F, Y, or W; and X₅=L or V. The homology in all the top binding clones occurred in the cyclic ring and not in the four amino acids flanking the cysteines.

One more round of maturation was carried out to further confirm all positions. The oligonucleotides for this library were designed as follows: CX₁FX₂GYDNX₃(X₄=F/Y/W)(X₅=L/V)C, where positions X₁ and X₃ were random; position X₂ expressed 50% Trp and 50% random amino acids; position X₄ expressed equimolar amounts of F, Y, and W; and position X₅ expressed equimolar amounts of L and V. This library was created with excellent diversity, having greater than 10 billion clones. Following three rounds of panning of this biased library on Grb7 protein, 96 clones were randomly picked for clone-binding analysis using phage ELISA.²⁵ In addition, the remaining eluate was subjected to further screening using a colony lift assay³¹ to the biotinylated Grb7. Colony lift assays are a way to screen large numbers of clones to identify rare high-affinity binding phage present in an excess of low-affinity clones. After the initial screening, the clones with the strongest signal were chosen for secondary screening in a colony lift assay, followed by sequencing and individual clone-binding analysis using phage ELISA. The binding

Fig. 1. The Grb7-SH2 structure in complex with G7-18NATE. (a) The sequence of the Grb7-SH2 domain with the secondary structural elements, as determined in the current structure, highlighted in rainbow colors. The archetypical SH2 domain secondary structural elements are shown schematically above with the naming system according to Eck *et al.*²⁹ Black dots above individual amino acids indicate residues that are involved in hydrogen-bond interactions with the G7-18NATE, and blue dots indicate residues that form part of the buried surface area. The aligned sequences and percentage identity of Grb14-SH2, Grb10-SH2, and Grb2-SH2 domains are shown for comparison. (b) A cartoon representation of the Grb7-SH2 domain with coloring correlated with that shown in (a). (c) The structure of the G7-18NATE peptide is shown in stick representation bound to the Grb7-SH2 domain. (d) Superposed cartoon structures of Grb7-SH2 bound to G7-18NATE (gray), the cocrystallized apo-Grb7-SH2 domain (orange), and the apo-Grb7-SH2 domain previously structurally determined (purple; PDB ID: 2QMS).

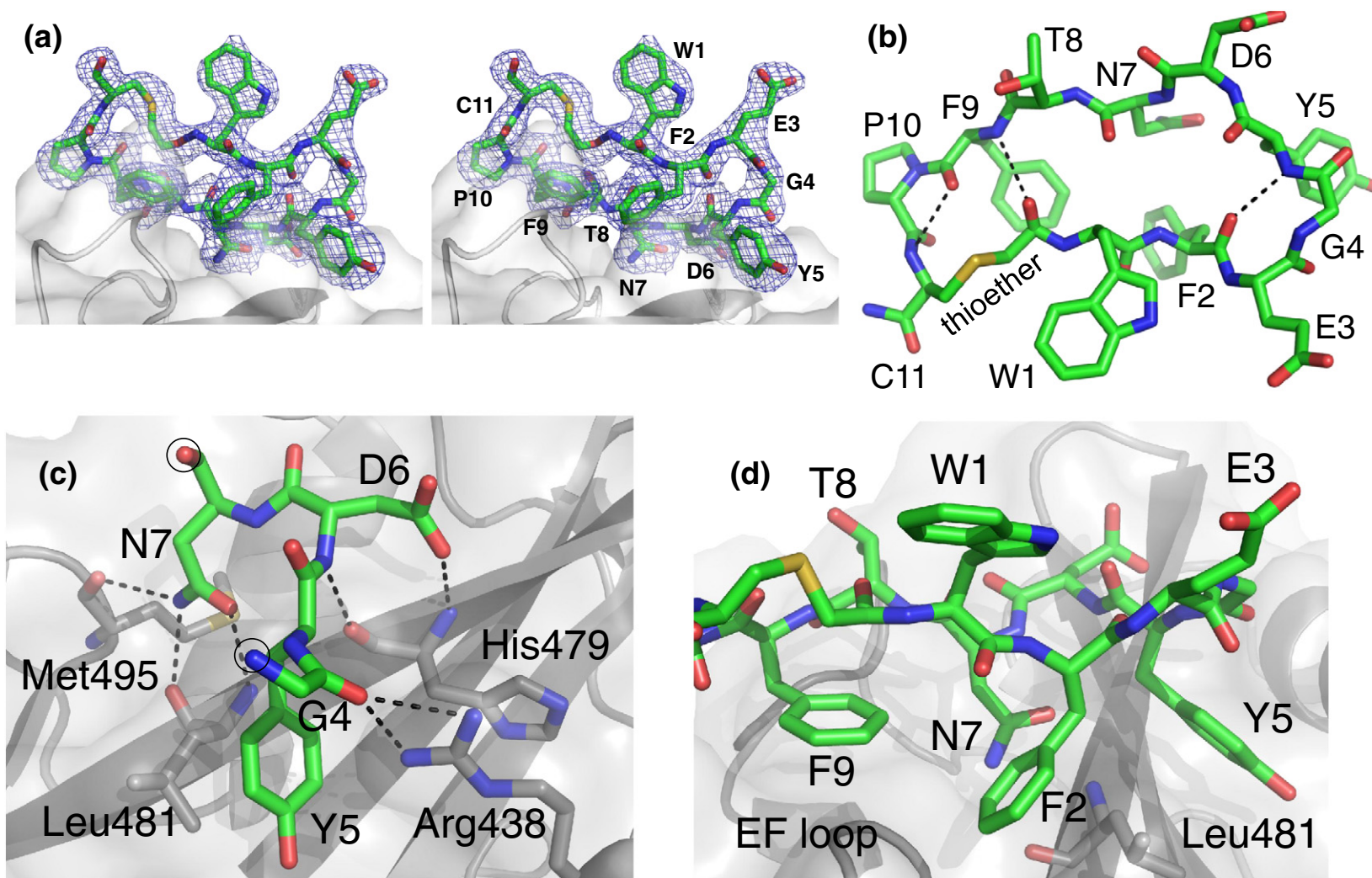


Fig. 2. The G7-18NATE structure in complex with the Grb7-SH2 domain. (a) Stereo diagram showing the $2F_o - F_c$ electron density map contoured at 1.2σ (blue mesh) that defines the structure of G7-18NATE at the surface of the Grb7-SH2 domain (gray). (b) G7-18NATE oriented to show intramolecular hydrogen bonds. (c) G7-18NATE amino acid residues from G4 to N7 (truncated ends of this segment are indicated with black circles) bound to the Grb7-SH2 domain. (d) The G7-18NATE molecule showing the positioning of aromatic amino acid residues F2 and F9 that form interactions with the Grb7-SH2 domain. In all images, G7-18NATE is shown in green stick representation, the Grb7-SH2 molecule is shown in gray cartoon representation with a transparent surface, and specific amino acids involved in interactions with the bound peptide are displayed in gray stick representation.

Table 1. The newly identified Grb7 binding clones identified from the YDN and YDN-NA biased libraries have sequence homology with each other and to our lead G7-18 peptide

G7-18	RSTLCW <u>F</u> <u>E</u> <u>G</u> <u>Y</u> <u>D</u> <u>N</u> <u>T</u> <u>F</u> PCKYFR
08-5367	CL <u>F</u> <u>W</u> <u>G</u> <u>Y</u> <u>D</u> <u>N</u> <u>E</u> <u>Y</u> <u>L</u> C
08-5073	LWLGCH <u>F</u> <u>A</u> <u>G</u> <u>Y</u> <u>D</u> <u>N</u> <u>E</u> <u>F</u> <u>L</u> CSRGG
08-5200	CA <u>F</u> <u>W</u> <u>G</u> <u>Y</u> <u>D</u> <u>N</u> W <u>V</u> C
08-5242	CI <u>F</u> <u>W</u> <u>G</u> <u>Y</u> <u>D</u> <u>N</u> SW <u>L</u> C

Identical and chemically similar amino acids (L, V and F, Y) are in boldface and underlined

of the individual clones were compared to G7-18 phage clone. Seventy-two of the strongest binding clones identified from random picking and colony lift analysis were grown and normalized using a plate-based assay developed in our laboratory for rapid quantification of phage for semi-high-throughput analysis.³² Figure 3 represents the sequences of the best binding clones as compared to G7-18 identified from this panning series. This affinity maturation identified a series of clones with strong binding. Multiple clones with identical sequences were also identified and are presented in Table 2. The conserved motif of these clones is CPFWGYDNEFLC, which is the exact sequence of clone 08-6110. However, clone 08-5992 differs by

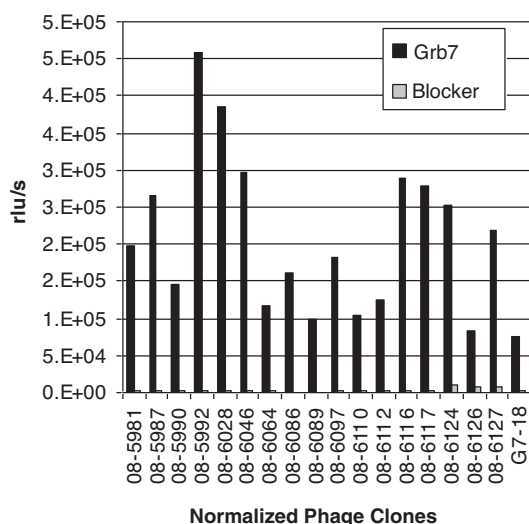


Fig. 3. Phage ELISA demonstrating the binding of the newly identified phage clones to the purified Grb7-SH2 domain. Equivalent amounts of phage were evaluated to determine their relative binding affinity to the SH2 domain of Grb7 as compared to our original G7-18 clone.²⁵ Phage were detected with anti-M13-HRP. The HRP was monitored with chemiluminescent substrate.

only one amino acid change, that is, from L to V at the X₅ position. 08-5992 repeatedly had better binding than 08-6110, indicating the value of V at the X₅ position. Clone 08-6028 had similar intensity of binding with clone 08-5992 and also shares the conserved motif with the exception at position X₃. The fourth clone of interest, 08-6046, which was narrowly the third highest binder in the ELISA assay, differed from the consensus sequence at positions X₂ and X₃. The notable feature of these peptides is the complete conservation of F2, G4, and F9 residues that, with the YDN motif, are precisely the amino acid residues that were found to form the basis for the binding interaction in the structural studies of the G7-18NATE/Grb7-SH2 complex.

These four peptides (08-5992, 08-6110, 08-6046, and 08-6028) were synthesized as thioether-cyclized peptides and analyzed for their binding affinity to the Grb7-SH2 domain as described below. In addition, peptides 08-5992 and 08-6028 were synthesized as free peptides conjugated to the Tat sequence and analyzed further to compare their antiproliferative properties to G7-18NATE-Tat. These newly identified peptides had the same level of antiproliferative activity as G7-18NATE-Tat in a BrdU chemiluminescent cell proliferation ELISA (Roche Applied Science, Indianapolis, IN) of SK-BR-3 breast cancer cells (data not shown).

Binding affinity of second-generation peptides

Using isothermal titration calorimetry (ITC), we and others have previously shown that G7-18NATE binds to the Grb7-SH2 domain with micromolar affinity.^{26,27,33,34} Using the same experimental conditions as previously conducted in our laboratory to arrive at a $K_d = 35 \mu\text{M}$ for G7-18NATE, we compared the binding of second-generation peptides 08-5992, 08-6110, 08-6046, and 08-6028. Similar to G7-18NATE, all peptides showed an exothermic heat of reaction (Fig. 4), although these varied between peptides as reflected in the different magnitudes of heat loss measured. Analysis of the curves allowed equilibrium dissociation constants (K_d) to be estimated (Table 3). K_d values were all found to be in the micromolar range (experiments were conducted in duplicate). Of these four peptides, 08-6046 displayed a slightly higher affinity than G7-18NATE with a $K_d = 18 \mu\text{M}$. The others were of similar or slightly lower affinity. Since none of these peptides bound with an affinity remarkably higher than that of the parent G7-18NATE, this demonstrates that the amino acids that vary between these peptides do not significantly have an impact on the binding interactions with the Grb7-SH2 domain. Conversely, these data show that the sum total of interactions underlying binding affinity is made by F2, G4, F9, and the YDN motif, in agreement with the crystal structure studies (Fig. 5).

Table 2. Sequence of clones identified from the CX₁FX₂GYDNX₃X₄X₅ library

Library design	No. of clones	C	X ₁	F	X ₂	G	Y	D	N	X ₃	X ₄	X ₅	C
		C	Random	F	50% W	G	Y	D	N	Random	33% FWY	50% L/V	
08-5992 ^a		C	P	F	W	G	Y	D	N	E	F	V	C
08-6116		C	M	F	W	G	Y	D	N	Q	F	L	C
08-6117		C	Q	F	W	G	Y	D	N	V	F	L	C
08-6028 ^a	9	C	P	F	W	G	Y	D	N	A	F	L	C
08-6127		C	L	F	W	G	Y	D	N	S	F	L	C
08-6124		C	P	F	F	G	Y	D	N	D	F	L	C
08-6097		C	L	F	G	G	Y	D	N	S	F	V	C
08-6086		C	K	F	G	G	Y	D	N	Q	W	L	C
08-5987	7	C	A	F	W	G	Y	D	N	A	F	L	C
08-6046 ^a		C	P	F	S	G	Y	D	N	Q	F	L	C
08-6112		C	L	F	Y	G	Y	D	N	A	F	L	C
08-6089		C	V	F	W	G	Y	D	N	Q	F	L	C
08-6110 ^a		C	P	F	W	G	Y	D	N	E	F	L	C
08-5990	5	C	Q	F	W	G	Y	D	N	D	F	L	C
08-5981	6	C	L	F	W	G	Y	D	N	E	F	L	C
08-6126		C	P	F	A	G	Y	D	N	W	F	L	C
08-6064		C	R	F	W	G	Y	D	N	S	F	L	C
Consensus		C	P	F	W	G	Y	D	N	E	F	L	C

Column 1 depicts the clone number, and column 2 depicts the number of clones with identical sequence. The amino acids that are italicized are those that were constant in this library, while those that are not italicized are those enriched for in this round of maturation.

^a Peptides further tested using ITC.

Discussion

The upregulation and overexpression of Grb7 in many cancers have a direct impact on their proliferative and metastatic potential. There is thus significant current interest in the development of Grb7 inhibitors that could be used in combating these cancers. The G7-18NATE peptide is the first peptide that has been discovered that binds with specificity to the Grb7-SH2 domain. Furthermore, cell-permeable forms of G7-18NATE have been shown to inhibit Grb7 interactions with binding partners *in vivo* and to reduce cancer cell migration and proliferation. The G7-18NATE thus represents an important starting point in the development of potent inhibitors that could be used in medical research and therapeutically. The current work has, therefore, been carried out in order to understand the structural basis for the G7-18NATE interaction with the Grb7-SH2 domain and to potentially identify peptides of enhanced affinity. While small-molecule inhibitor development may also represent a path to targeting Grb7, no small-molecule inhibitor with specificity or high affinity has been discovered to date, although we are also pursuing this approach.³⁵

The crystal structure of the G7-18NATE/Grb7-SH2 domain complex reported here reveals the structural basis for their interaction. It is remarkable that the G7-18NATE peptide binds to the Grb7-SH2 domain with micromolar affinity despite being nonphosphorylated. The binding interaction is, in part, assisted by the peptide being cyclized to constrain the peptide. It has been shown that the linear form of the peptide does not bind with detectable affinity.²⁵ Cyclization is presumed to

reduce the loss of conformational entropy upon binding. We have previously reported that the G7-18NATE peptide has a propensity to adopt a turn about the YDN motif,³⁶ and the current Grb7-SH2/G7-18NATE structure confirms that, indeed, the G7-18NATE peptide adopts the anticipated turn when bound to its target. The YDN motif is positioned precisely where analogous YXN motifs are positioned, bound to both Grb2-SH2 and Grb7-SH2 domains,^{30,37} forming van der Waals and hydrogen-bond interactions about the β D6 residue Leu481, as was predicted in our modeling studies.²⁶ At the phosphotyrosine binding site of the Grb7-SH2 domain, arginine residues (Arg438 and Arg458), which would be expected to form hydrogen-bond interactions with the phosphate of the phosphotyrosine of a physiological substrate, are engaged in interactions with the G4 backbone carbonyl and, in this crystal form, with the E3 glutamic acid side chain from an adjacent G7-18NATE/Grb7-SH2 domain complex. This explains the selection of a glycine, since it uniquely possesses the conformational flexibility required for the interaction. It raises the question, however, of whether the E3 side chain would be positioned differently in solution, possibly even playing a role in G7-18NATE binding. This answer is provided through the phage display work, discussed further below, in which a glutamic acid was not selected from the peptide libraries. It is therefore unlikely to play a role in the primary G7-18NATE interaction with the Grb7-SH2 domain but may have assisted with the crystal formation. An important additional contribution to G7-18NATE binding arises from the positioning of two phenylalanine residues (F2 and F9) that contribute to van

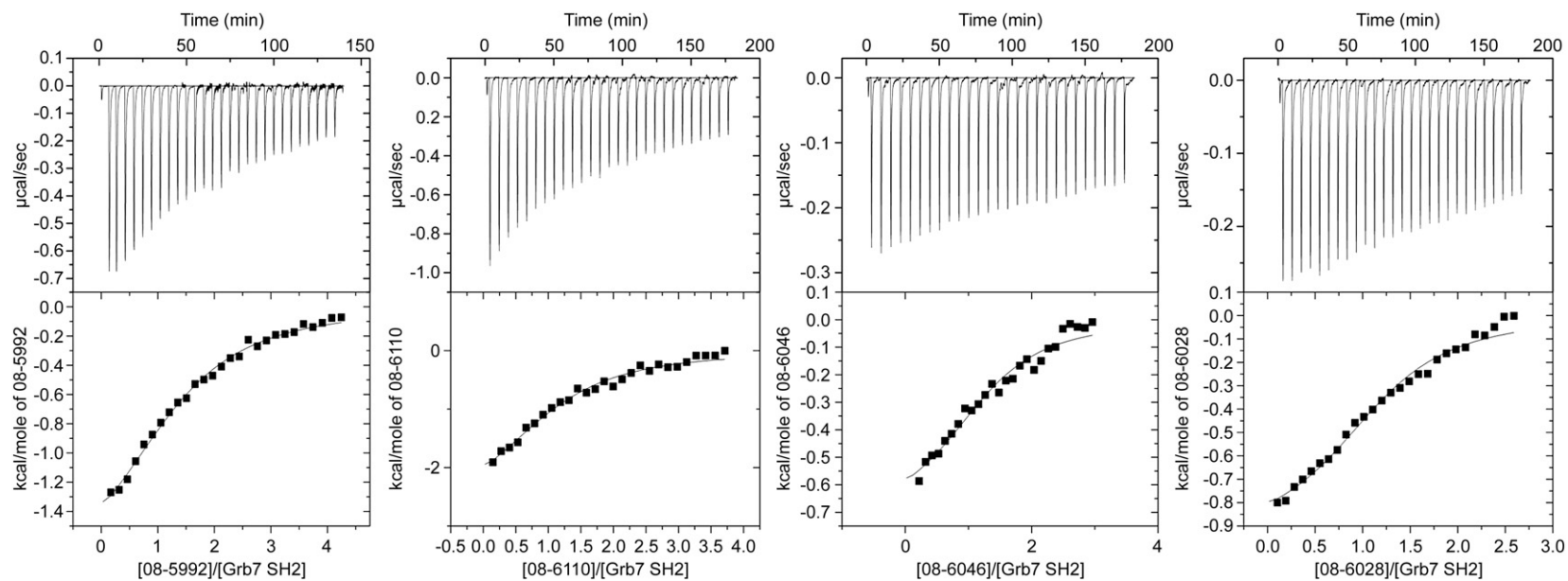


Fig. 4. Binding of second-generation G7-18NATE peptides to the Grb7-SH2 domain. ITC thermograms obtained from the isothermal titration of G7-18NATE analogues (08-5992, 08-6110, 08-6046, and 08-6028) against the Grb7-SH2 domain. The upper panels show raw data obtained from 10- μ l injections of peptides at 25 $^{\circ}$ C. The lower panels display plots of integrated total energy exchanged (as kilocalories per mole of injected peptides) as a function of molar ratio of the peptides to the Grb7-SH2 domain.

Table 3. Thermodynamic binding parameters of G7-18NATE analogues

Binding parameter	08-5992	08-6110	08-6046	08-6028
<i>N</i>	1.2±0.18	1.13±0.09	1.31±0.08	1.05±0.162
<i>K</i> (10 ⁴ M ⁻¹)	1.73±0.23	2.26±0.47	5.53±0.14	1.91±0.40
ΔH (kcal mol ⁻¹)	-1.92±0.37	-2.89±0.33	-1.64±0.06	-1.60±0.33
$-T\Delta S$ (kcal mol ⁻¹)	-3.83	-3.05	-5.83	-4.23
ΔG (kcal mol ⁻¹)	-5.75±0.37	-5.94±0.33	-6.48±0.06	-5.84±0.33
<i>K_d</i> (μM)	57.8	44.25	18.1	52.36

der Waals interactions with the Grb7-SH2 domain, extending the total surface area of interaction to 458 Å².

The interaction formed between the G7-18NATE peptide and the Grb7-SH2 domain bears some resemblance to other ligand SH2 domain interactions and possesses some unique features. Besides the YXN motif interactions, the positioning of an aromatic residue against the βD6 side chain (as seen for F2 in the current structure) has similarly been observed for ligands bound to the Grb2-SH2 domain.^{38,39} The G7-18NATE interaction with the Grb7-SH2 domain is, however, unlike that reported for the one other ligand-bound structure of the Grb7-SH2 domain. The structure of a 10-residue phosphorylated peptide, representing the pY1339 target site of the erbB-2 receptor, bound to the Grb7-SH2 domain has been solved using NMR spectroscopy³⁷ (PDB IDs: 1MW4 and 2L4K). In this structure, although the YXN motif is positioned similarly, the rest of the peptide is positioned at a different surface interface from that adopted by G7-18NATE. No residues are positioned similarly to the G7-18NATE F2 (against the βD6 side chain) or F9 (over the EF loop). In fact, the structures of the Grb7-SH2 domain DE and EF loops are dramatically repositioned by the pY1339 ligand interaction for reasons that are, as yet, unclear.

It is of interest that, in this crystal form, the G7-18NATE is bound to the Grb7-SH2 domain in a 1:2 stoichiometric ratio, with only one SH2 domain of every Grb7-SH2 domain dimer bound by peptide. This is most likely due to the packing arrangement of this crystal form in which every second G7-18NATE binding site is occluded. Previous solution studies using analytical ultracentrifugation and ITC have shown that a Grb7-SH2 domain dimer forms in solution and interacts with G7-18NATE in a 1:1 stoichiometric ratio—that is, with a G7-18NATE peptide bound to every available SH2 domain.^{26,33,34}

The structure provides insight into the basis of specificity of G7-18NATE for the Grb7-SH2 domain over SH2 domains of Grb14, Grb10, and Grb2. The interaction with Leu481 is understood to form the basis for specificity of peptide binding to the Grb7-SH2 domain, with a mutation made to Leu481 being enough to completely abrogate binding or the addition of Leu481 to the Grb14-SH2 domain being enough to confer binding.⁴⁰ While the equivalent experiment has not been carried out for G7-18NATE, the central importance of Leu481 is clearly seen for G7-18NATE binding to the Grb7-SH2 domain. Not only is the Y5 side chain positioned over the Leu481 side chain and the N7 side chain hydrogen bonded to the Leu481 backbone groups, but the F2 side chain is also positioned against the Leu481 side chain. Any changes to this residue would be expected to disrupt these optimized interactions. Other interactions made by G7-18NATE are with amino acid residues that are conserved across Grb14, Grb10, and Grb2 or with amino acid backbone functionalities, and it is thus unlikely that these interactions underlie specificity.

Two phage display libraries were employed to generate second-generation peptides with affinity for the Grb7-SH2 domain. These maintained the YDN motif and established its importance for G7-18NATE binding. Enriched peptides were screened for Grb7-SH2 domain binding using an ELISA-based assay, from which four new peptides that bind to the Grb7-SH2 domain were discovered. This established the importance of F5 and G4 before the YDN motif and an aromatic and hydrophobic residue after the YDN motif. In a further maturation step that maintained this consensus pattern, a

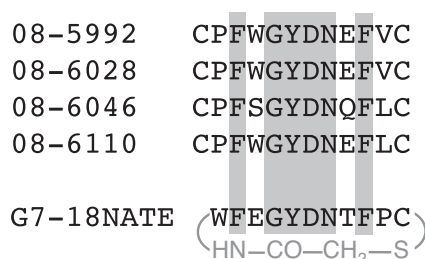


Fig. 5. Sequences of second-generation G7-18NATE peptides. Shown are the sequences of four second-generation peptides that were developed using phage display and further tested as thioether-cyclized peptides using ITC. Highlighted in red are the amino acid residues that were conserved among the Grb7-SH2 domain binding sequences. These residues correspond exactly to the residues shown to be structurally important for binding.

library of over 10 billion clones was screened for an optimized binder. Multiple clones were identified as strong binders relative to the G7-18NATE sequence in the ELISA-based assay. A notable feature of these peptides is the almost complete conservation of F2, G4, and F9 residues that, with the YDN motif, are precisely the amino acid residues that the G7-18NATE/Grb7-SH2 structure revealed to form the basis for the binding interaction.

Four of the second-generation peptides were synthesized as thioether-cyclized peptides by analogy to the G7-18NATE peptide. These all displayed similar micromolar binding for the Grb7-SH2 domain. In all cases, their equilibrium dissociation constants (K_d values) were in the micromolar range (18–52 μM), similar to that found for G7-18NATE (35 μM). No second-generation peptide displayed a significantly enhanced affinity for the Grb7-SH2 domain despite the apparent higher affinity of the ELISA-screened phage-displayed peptides. In view of the structural data, this is not unexpected. The differences between the second-generation peptides and G7-18NATE occur exclusively at the amino acid residue positions that, as the structural data show, do not interact with the Grb7-SH2 domain. The peptides are completely conserved at the amino acid residues that form the basis for the interaction. Together, the data suggest that this class of cyclic peptide, with the consensus motif XFXGYDNXFXX, has been optimized for interaction with the Grb7-SH2 domain.

Conclusion

This study has revealed the basis for interaction of the G7-18NATE peptide with its Grb7-SH2 domain target, which will greatly assist in the development of inhibitors against Grb7 in cancer. The crystal structure of the Grb7-SH2/G7-18NATE complex has revealed the mode of interaction and the identity of the key functionalities that interact with the target. Peptide sequences derived from phage display methods contained these key residues. They displayed similar and better binding affinity to the target but did not represent a significantly improved peptide for Grb7-SH2 inhibition. Together, this suggests that the key amino acids that form the basis for the interaction have been optimized for this class of cyclic-peptide binding to the Grb7-SH2 domain. It can be concluded that further improvements to the affinity of interaction will not be made by substitution of the common amino acids at any position but will require other strategies, such as the incorporation of nonnatural amino acids or the preparation of constrained G7-18NATE analogues that retain the key interactions. Such investigations are the focus of our current research.

Materials and Methods

Grb7-SH2 domain preparation

Expression and purification of the SH2 domain of Grb7 (residues 415–532) were conducted using established protocols.^{26,41} In brief, the SH2 domain was overexpressed as a glutathione *S*-transferase fusion protein in the *Escherichia coli* strain BL21(DE3)pLysS. After affinity purification using glutathione resin, the glutathione *S*-transferase was cleaved using thrombin and the protein was further purified using cation- and size-exclusion chromatography. Purity was determined using SDS-PAGE, and the protein was concentrated to 10 mg/ml as determined spectrophotometrically at 280 nm using an extinction coefficient of 8480 M^{-1} . The final purified construct comprised residues 415–532 of Grb7 preceded by the amino acid residues GS.

Peptide synthesis

The G7-18NATE and analogues were synthesized as peptide amides using the Fmoc-based solid-phase peptide synthesis strategy on a rink amide resin (1.0 mmol/g). Details are as reported previously for the synthesis of G7-18NATE.^{26,34} The following peptide sequences were synthesized: WFEGYDNTFPC (G7-18NATE), PFWGYDNEFVC (08-5992), PFWGYDNEFVC (08-6028), PFSGYDNQFLC (08-6110), and PFWGYDNEFLC (08-6046). Following incorporation of the residues using the microwave synthesizer (CEM Liberty System; CEM, Matthews, NC) and removal of the final Fmoc group, *N*-terminal chloroacetylation was carried out using 171 mg of chloroacetic anhydride, 2 ml of dimethylformamide, and 100 μl of diisopropylethylamine. The reaction was carried out manually at room temperature for 30 min. The dried peptide was then cleaved and fully deprotected using a cocktail of 94.5% trifluoroacetic acid/2.5% triisopropylsilane/2.5% H_2O /0.5% ethane dithiothreitol in a 20-fold excess volume over dry weight of resin peptide for 3 to 4 h at room temperature. After workup, thioether formation was effected by dissolving the lyophilized peptide at 2 mg/ml in 50 mM NH_4HCO_3 in 50% acetonitrile/ H_2O , pH 8.0, for 1.5 h at room temperature. The success of cyclization was followed by mass spectrometry. The cyclized peptides were purified using preparative reversed-phase HPLC, and their successful preparation was confirmed using electrospray mass spectrometry in negative ion mode (average molecular masses are listed) (G7-18NATE: $M_{\text{expected}} = 1417.6$, $M_{\text{observed}} = 1417.1$; 08-5992: $M_{\text{expected}} = 1415.0$, $M_{\text{observed}} = 1415.4$; 08-6028: $M_{\text{expected}} = 1370.6$, $M_{\text{observed}} = 1370.8$; 08-6110: $M_{\text{expected}} = 1428.6$, $M_{\text{observed}} = 1429.0$; 08-6046: $M_{\text{expected}} = 1328.5$, $M_{\text{observed}} = 1328.8$).

Crystallization of the Grb7-SH2/G7-18NATE complex and data collection

The crystallization and diffraction data collection for the Grb7-SH2/G7-18NATE complex have been previously reported.⁴¹ In brief, the Grb7-SH2 protein, concentrated to 10 mg/ml and in 4-morpholineethanesulfonic acid buffer,

Table 4. Data refinement parameters

Grb7-SH2/G7-18NATE	
<i>Data collection</i> ^a	
Space group	$P2_1$
Cell dimensions	
<i>a</i> , <i>b</i> , <i>c</i> (Å)	52.7, 79.1, 54.7
α , β , γ (°)	90.0, 104.4, 90.0
Resolution (Å)	37.42–2.41 (2.48–2.41)
R_{merge} (%)	9.6 (43.2)
$I/\sigma I$	7.3 (2.0)
Reflections measured	16,204 (unique)
Completeness (%)	96.1 (86.3)
Redundancy	4.1 (3.6)
<i>Refinement</i>	
Resolution (Å)	2.41
No. of reflections used	16,204 (unique)
$R_{\text{work}}/R_{\text{free}}$	23.7/27.7
No. of atoms	
Protein	3227
Peptide	200
Ions	0
Water	116
<i>B</i> -factors (Å ²)	
Protein	34.0
Peptide	26.7
Ions	—
Water	32.1
RMSDs	
Bond lengths (Å)	0.010
Bond angles (°)	1.2
Ramachandran plot ^c (%)	
Favored regions	95.7
Allowed regions	99.0

^a Values in parentheses refer to the highest-resolution shell.

^b $R_{\text{merge}} = \sum |I - \langle I \rangle| / \sum \langle I \rangle$, where *I* is the intensity of individual reflections.

^c Determined using the program MolProbity.⁴³

was added to lyophilized peptide to achieve a 1:2 protein-to-peptide ratio. The mixture formed crystals in a 2- μ l hanging drop using 17.5% (w/v) polyethylene glycol 3350, 0.2 M magnesium chloride hexahydrate, 0.1 M glycine, 10% (w/v) glycerol, and 0.1 M 2-[bis(2-hydroxyethyl)amino]-2-(hydroxymethyl)propane-1,3-diol, pH 6.0, as the precipitant solution. The crystals formed as small thin plates (approximately 0.01 mm \times 0.06 mm \times 0.1 mm in size) over 2 days and, after cryo-freezing, diffracted to 2.4 Å resolution. X-ray diffraction data were collected on the high-throughput protein (MX1) crystallography beamline at the Australian Synchrotron. X-ray diffraction data were integrated and scaled with XIA2.⁴² The crystallographic data and refinement statistics are reported in Table 4. The diffraction data were consistent with space group $P2_1$ with unit cell dimensions $a=52.7$ Å, $b=79.1$ Å, $c=54.7$ Å, $\alpha=90.0$, $\beta=104.4$, and $\gamma=90.0$ and collected with a completeness of 96.1% from 37.42 to 2.41 Å resolution (86.3% in the highest-resolution bin from 2.48 to 2.41 Å resolution).

Structure determination of the Grb7-SH2/G7-18NATE complex

The structure of the Grb7-SH2/G7-18NATE complex was solved using the molecular replacement method.

Initial phases were obtained using MOLREP⁴⁴ and the coordinates of the apo-Grb7-SH2 structure previously determined in our laboratory (PDB ID: 2QMS) as the search model. The correct solution had a correlation coefficient of 67.7 and an *R*-factor of 46.8, whereas the next unrelated peak had a correlation coefficient of 55.1 and an *R*-factor of 54.8. Manual model rebuilding was carried out using Coot,⁴⁵ and maximum likelihood refinement was carried out using PHENIX.⁴⁶ Noncrystallographic symmetry restraints were applied between pairs of chains that occupied the asymmetric unit but were removed for the final round of refinement. Successive rounds of refinement and manual building were performed. The refinement statistics are reported in Table 4. The program MolProbity⁴³ was used to assess the quality of the final structures (99% of the amino acids possess backbone torsional angles within the allowed regions of the Ramachandran plot).

The final G7-18NATE/Grb7-SH2 complex structure solved to 2.4 Å resolution consists of four chains of the Grb7-SH2 domain and two G7-18NATE molecules in the asymmetric unit. The crystal is composed of Grb7-SH2 dimers in which one monomer of each dimer is peptide bound (chains A and B) and the other is apo-Grb7-SH2 (chains C and D). The final model also contains 116 water molecules and has an *R*-factor of 23.7% ($R_{\text{free}}=27.7\%$) (Table 4). Interpretable electron density was present for residues 423–529 but was missing for the 10 N-terminal residues of the construct (GSPASGTSLS) and the last 3 residues (VAL). Some disorder was also observed at residues 460–464 and 487–489 that occur at loop regions. The four chains did not significantly differ from each other with C^α RMSDs of 0.32 Å (A/B holo-chains across 106 atoms) and 0.21 Å (C/D apo-chains) between like chains and C^α RMSDs of 0.54 Å (A/C) and 0.54 Å (A/D) between unlike chains (across 96 atoms). The whole of the G7-18NATE peptide was clearly visible in the electron density map. The coordinates have been deposited at the Research Collaboratory for Structural Bioinformatics database (PDB ID: 3PQZ).

Phage library construction

The peptide biased libraries used in these studies were constructed in the fUSE5 gene III phage-display system⁴⁷ according to the methods previously reported.²⁵ The fUSE5 vector (K91 Kan) and *E. coli* host (MC1061F') strains were generous gifts of Dr. George Smith at the University of Missouri. There were two rounds of library construction. The half-site cloning method used by Cwirla *et al.* was employed in the construction of these libraries.⁴⁸ The two "half-site" oligos 5'tccgcagcccgct3' (GS5') and 5'cgccccgctcc3' (GS3') are complementary to the 5' and 3' ends of the peptide-insert-encoding oligonucleotide, respectively. The random peptide-encoding oligonucleotides for the first round of libraries have the following sequences for the YDN-NA biased library and the YDN biased library, respectively: 5'gggcccggaggatga(NNK)₄tatgacaat(NNK)₃-tgccggggccgctg3' and 5'gggcccggaggatga(NNK)₄tga(NNK)₄-tatgacaat(NNK)₃tgcc(NNK)₄ggggccgctg3' (N=equal amounts of G, A, T, or C; K=equal amounts of G or T). The random peptide-encoding oligonucleotides for the second round of library construction have the

following sequence: 5'tattctcactcgccgacggggccggaggatgc NNNKttc123ggttacgacaacNNK456789tcggggccgctggggcc-gaaactgttc3' (where N and K are the same as noted above). The oligonucleotide denoted "123" is designed (1=12.5% G, 12.5% A, 62.5% T, 12.5% C; 2=62.5% G, 12.5% A, 12.5% T, 12.5% C; 3=66.6% G, 33.3% T) to obtain 50% of the clones expressing random amino acids and the rest expressing tryptophan at this position. The oligonucleotide denoted "456" is designed (4=100% T; 5=33.3% G, 33.3% A, 33.3% T; 6=33.3% G, 66.6% C) to randomize Phe, Tyr, or Trp at this position. The oligonucleotide denoted "789" is designed (7=50% G, 50% C; 8=100% T; 9=50% G, 50% T) to express Leu or Val at this position. All oligonucleotides were synthesized by Biosynthesis Inc. (Lewisville, TX).

Phage library screening

The methods for panning the newly created biased libraries against the target and clone-binding analysis using phage ELISA have been previously reported.²⁵ The only modification made here was the use of SuperSignal ELISA Femto chemiluminescent substrate (Pierce, Rockford, IL) instead of ABTS for measuring the horseradish peroxidase (HRP)-conjugated anti-M13 antibody (Amersham) using a chemiluminescent plate reader (GloRunner, Turner BioSystems, Sunnyvale, CA). In order to achieve an equivalent phage input in the binding studies, we carried out normalization of the phage preparations using the Chemiluminescent ELISA methods developed in our laboratory.³² The colony lift assays were performed as previously described.³¹ The vector DNA of each selected clone was purified using QIAprep Spin Miniprep Kit (Qiagen, Inc., Chatsworth, CA) according to the manufacturer's instructions. The pIII sequencing primer, 5-CCC TCA TAG TTA GCG TAA CG-3, designed by Dr. George Smith, was used for sequencing the DNA inserts. The sequence reactions were carried out using BigDye Ver 3.1 Dye Terminator kit (Life Technologies, Foster City, CA) by the Vermont Cancer Center DNA Analysis Facility.

ITC determination of peptide-protein affinities

For ITC experiments, the Grb7-SH2 domain protein was dialyzed against sodium acetate buffer (50 mM NaOOCCH₃, 100 mM NaCl, and 1 mM NaN₃, pH 6.6). The filtered dialysate buffer was used to dilute the required amount of the Grb7-SH2 domain to a volume of 2.5 ml and a concentration of 40 to 85 μM. Lyophilized peptide of accurately determined mass was dissolved in 500 μl of the filtered dialysate buffer. The peptide concentrations employed were 10 to 30 times higher than the protein concentration. Following this, both the peptide and the Grb7-SH2 domain solutions were degassed for 5 min. ITC experiments were conducted using a VP-ITC MicroCalorimeter (MicroCal, Northampton, MA). All experiments were performed in duplicate at 25 °C cell temperature, and the total number of injections was set to 30 with volume injections of 10 μl, an injection duration of 20 s, and an injection interval of 250 to 400 s. The reference power was set at 20 μcal/s, and the initial injection delay was 60–70 s. The stirring speed was 307 rpm, and the feedback mode gain was set to high with the fast and auto equilibration options applied. A

binding isotherm was generated by plotting the heat change evolved per injection against the molar ratio of peptides to the Grb7-SH2 domain receptor. A blank determination in which the peptides were titrated against the buffer was carried out to account for heats of dilution and mixing, which was then subtracted from the binding data. The corrected data were then employed to fit to a single binding site model using the nonlinear least-squares fitter from Origin (MicroCal Software, Northampton, MA). All of the ITC fitting parameters were kept floating.

Accession numbers

Coordinates and structure factors have been deposited in the PDB with accession number 3PQZ.

Acknowledgements

We wish to thank the staff at the Protein Crystallography Beamline (MX1) at the Australian Synchrotron, Victoria, Australia, where the diffraction data were collected. This work was funded by an Australian Research Council Project Grant awarded to J.A.W. and D.N.K., a Monash University Graduate Scholarship awarded to N.D.A., and a National Health and Medical Research Senior Research Fellowship awarded to M.C.J.W. The automated DNA sequencing was performed at the Vermont Cancer Center DNA Analysis Facility and was supported by Vermont Cancer Center, Lake Champlain Cancer Research Organization, and the University of Vermont College of Medicine. The phage display work was funded by the National Cancer Institute (R01 CA80790) and in part by the SD Ireland Cancer Research Foundation.

References

1. Han, D. C., Shen, T. L. & Guan, J. L. (2001). The Grb7 family proteins: structure, interactions with other signaling molecules and potential cellular functions. *Oncogene*, **20**, 6315–6321.
2. Shen, T. L. & Guan, J. L. (2004). Grb7 in intracellular signaling and its role in cell regulation. *Front. Biosci.* **9**, 192–200.
3. Manser, J., Roonprapunt, C. & Margolis, B. (1997). *C. elegans* cell migration gene mig-10 shares similarities with a family of SH2 domain proteins and acts cell nonautonomously in excretory canal development. *Dev. Biol.* **184**, 150–164.
4. Stein, D., Wu, J., Fuqua, S. A., Roonprapunt, C., Yajnik, V., D'Eustachio, P. *et al.* (1994). The SH2 domain protein GRB-7 is co-amplified, overexpressed and in a tight complex with HER2 in breast cancer. *EMBO J.* **13**, 1331–1340.
5. Tanaka, S., Mori, M., Akiyoshi, T., Tanaka, Y., Mafune, K., Wands, J. R. & Sugimachi, K. (1997).

- Coexpression of Grb7 with epidermal growth factor receptor or Her2/erbB2 in human advanced esophageal carcinoma. *Cancer Res.* **57**, 28–31.
6. Kishi, T., Sasaki, H., Akiyama, N., Ishizuka, T., Sakamoto, H., Aizawa, S. *et al.* (1997). Molecular cloning of human GRB-7 co-amplified with CAB1 and c-ERBB-2 in primary gastric cancer. *Biochem. Biophys. Res. Commun.* **232**, 5–9.
 7. Wang, Y., Chan, D. W., Liu, V. W. S., Chiu, P. & Ngan, H. Y. S. (2010). Differential functions of growth factor receptor-bound protein 7 (GRB7) and its variant GRB7v in ovarian carcinogenesis. *Clin. Cancer Res.* **16**, 2529–2539.
 8. Walch, A., Specht, K., Braselmann, H., Stein, H., Siewert, J., Hopt, U. *et al.* (2004). Coamplification and coexpression of GRB7 and ERBB2 is found in high grade intraepithelial neoplasia and in invasive Barrett's carcinoma. *Int. J. Cancer*, **112**, 747–753.
 9. Itoh, S., Taketomi, A., Tanaka, S., Harimoto, N., Yamashita, Y. I., Aishima, S. I. *et al.* (2007). Role of growth factor receptor bound protein 7 in hepatocellular carcinoma. *Mol. Cancer Res.* **5**, 667–673.
 10. Nadler, Y., González, A. M., Camp, R. L., Rimm, D. L., Kluger, H. M. & Kluger, Y. (2010). Growth factor receptor-bound protein-7 (Grb7) as a prognostic marker and therapeutic target in breast cancer. *Ann. Oncol.* **21**, 466–473.
 11. Ramsey, B., Bai, T., Hanlon Newell, A., Troxell, M., Park, B., Olson, S. *et al.* (2011). GRB7 protein overexpression and clinical outcome in breast cancer. *Breast Cancer Res. Treat.* **127**, 659–669.
 12. Kao, J. & Pollack, J. (2006). RNA interference-based functional dissection of the 17q12 amplicon in breast cancer reveals contribution of coamplified genes. *Genes Chromosomes Cancer*, **45**, 761–769.
 13. Nencioni, A., Cea, M., Garuti, A., Passalacqua, M., Raffaghello, L., Soncini, D. *et al.* (2010). Grb7 upregulation is a molecular adaptation to HER2 signaling inhibition due to removal of Akt-mediated gene repression. *PLoS One*, **5**, e9024.
 14. Bai, T. & Luoh, S. W. (2008). GRB-7 facilitates HER-2/Neu-mediated signal transduction and tumor formation. *Carcinogenesis*, **29**, 473–479.
 15. Han, D. C. & Guan, J. L. (1999). Association of focal adhesion kinase with Grb7 and its role in cell migration. *J. Biol. Chem.* **274**, 24425–24430.
 16. Han, D. C., Shen, T. L. & Guan, J. L. (2000). Role of Grb7 targeting to focal contacts and its phosphorylation by focal adhesion kinase in regulation of cell migration. *J. Biol. Chem.* **275**, 28911–28917.
 17. Tanaka, S., Pero, S. C., Taguchi, K., Shimada, M., Mori, M., Krag, D. N. & Arai, S. (2006). Specific peptide ligand for Grb7 signal transduction protein and pancreatic cancer metastasis. *J. Natl. Cancer Inst.* **98**, 491–498.
 18. Pero, S. C., Daly, R. J. & Krag, D. N. (2003). Grb7-based molecular therapeutics in cancer. *Expert Rev. Mol. Med.* **5**, 1–11.
 19. Daly, R. J. (1998). The Grb7 family of signalling proteins. *Cell. Signalling*, **10**, 613–618.
 20. Chu, P. Y., Huang, L. Y., Hsu, C. H., Liang, C. C., Guan, J. L., Hung, T. H. & Shen, T. L. (2009). Tyrosine phosphorylation of growth factor receptor-bound protein-7 by focal adhesion kinase in the regulation of cell migration, proliferation, and tumorigenesis. *J. Biol. Chem.* **284**, 20215–20226.
 21. Tsai, N., Bi, J. & Wei, L. (2007). The adaptor Grb7 links netrin-1 signaling to regulation of mRNA translation. *EMBO J.* **26**, 1522–1531.
 22. Holt, L. J. & Daly, R. J. (2005). Adapter protein connections: the MRL and Grb7 protein families. *Growth Factors*, **23**, 193–201.
 23. Chu, P. Y., Li, T. K., Ding, S. T., Lai, I. R. & Shen, T. L. (2010). EGF-induced Grb7 recruits and promotes Ras activity essential for the tumorigenicity of Sk-Br3 breast cancer cells. *J. Biol. Chem.* **285**, 29279–29285.
 24. Tsai, N. P., Ho, P. C. & Wei, L. N. (2008). Regulation of stress granule dynamics by Grb7 and FAK signalling pathway. *EMBO J.* **27**, 715–726.
 25. Pero, S. C., Oligino, L., Daly, R. J., Soden, A. L., Liu, C., Roller, P. P. *et al.* (2002). Identification of novel non-phosphorylated ligands, which bind selectively to the SH2 domain of Grb7. *J. Biol. Chem.* **277**, 11918–11926.
 26. Porter, C. J., Matthews, J. M., Mackay, J. P., Pursglove, S. E., Schmidberger, J. W., Leedman, P. J. *et al.* (2007). Grb7 SH2 domain structure and interactions with a cyclic peptide inhibitor of cancer cell migration and proliferation. *BMC Struct. Biol.* **7**, 58.
 27. Gunzburg, M., Ambaye, N., Del Borgo, M., Hertzog, J., Pero, S., Krag, D. *et al.* (2010). Use of SPR to study the interaction of G7-18NATE peptide with the Grb7-SH2 domain. *Int. J. Pept. Res. Ther.* **16**, 177–184.
 28. Pero, S. C., Shukla, G. S., Cookson, M. M., Flemer, S. & Krag, D. N. (2007). Combination treatment with Grb7 peptide and Doxorubicin or Trastuzumab (Herceptin) results in cooperative cell growth inhibition in breast cancer cells. *Br. J. Cancer*, **96**, 1520–1525.
 29. Eck, M., Shoelson, S. & Harrison, S. (1993). Recognition of a high-affinity phosphotyrosyl peptide by the Src homology-2 domain of p56lck. *Nature*, **362**, 87–91.
 30. Rahuel, J., Gay, B., Erdmann, D., Strauss, A., Garcia-Echeverria, C., Furet, P. *et al.* (1996). Structural basis for specificity of Grb2-SH2 revealed by a novel ligand binding mode. *Nat. Struct. Biol.* **3**, 586–589.
 31. Sparks, A., Adey, N., Cwirla, S. & Kay, B. (1996). Screening phage-displayed random peptide libraries. In *Phage Display of Peptides and Proteins, a Laboratory Manual* (Kay, B. K., Winter, J. & McCafferty, J., eds), pp. 227–253, Academic Press, Inc., San Diego, CA.
 32. Shukla, G. & Krag, D. (2005). A sensitive and rapid chemiluminescence ELISA for filamentous bacteriophages. *J. Immunoassay Immunochem.* **26**, 89–95.
 33. Spuches, A. M., Argiros, H. J., Lee, K. H., Haas, L. L., Pero, S. C., Krag, D. N. *et al.* (2007). Calorimetric investigation of phosphorylated and non-phosphorylated peptide ligand binding to the human Grb7-SH2 domain. *J. Mol. Recognit.* **20**, 245–252.
 34. Ambaye, N. D., Lim, R. C. C., Clayton, D. J., Gunzburg, M. J., Price, J. T., Pero, S. C. *et al.* (2011). Uptake of a cell permeable G7-18NATE construct into cells and binding with the Grb7-SH2 domain. *Biopolymers*, **96**, 181–188.
 35. Ambaye, N., Gunzburg, M., Lim, R., Price, J., Wilce, M. & Wilce, J. (2011). Benzopyrazine derivatives: a novel class of growth factor receptor bound protein 7 antagonists. *Bioorg. Med. Chem.* **19**, 693–701.
 36. Porter, C. & Wilce, J. (2007). NMR analysis of G7-18NATE, a nonphosphorylated cyclic peptide

- inhibitor of the Grb7 adapter protein. *Biopolymers*, **88**, 174–181.
37. Ivancic, M., Daly, R. & Lyons, B. (2003). Solution structure of the human Grb7-SH2 domain/erbB2 peptide complex and structural basis for Grb7 binding to ErbB2. *J. Biomol. NMR*, **27**, 205–219.
 38. Phan, J., Shi, Z., Burke, T. & Waugh, D. (2005). Crystal structures of a high-affinity macrocyclic peptide mimetic in complex with the Grb2 SH2 domain. *J. Mol. Biol.* **353**, 104–115.
 39. Ogura, K., Shigam, T., Yokochi, M., Yuzawa, S., Burke, T. & Inagaki, F. (2008). Solution structure of the Grb2 SH2 domain complexed with a high-affinity inhibitor. *J. Biomol. NMR*, **42**, 197–207.
 40. Janes, P. W., Lackmann, M., Church, W. B., Sanderson, G. M., Sutherland, R. L. & Daly, R. J. (1997). Structural determinants of the interaction between the erbB2 receptor and the Src homology 2 domain of Grb7. *J. Biol. Chem.* **272**, 8490–8497.
 41. Yap, M., Wilce, M., Clayton, D., Perlmutter, P., Aguilar, M. I. & Wilce, J. A. (2010). Preparation and crystallization of the Grb7-SH2 domain in complex with the G7-18NATE non-phosphorylated cyclic inhibitor peptide. *Acta Crystallogr., Sect. F: Struct. Biol. Cryst. Commun.* **66**, 1640–1643.
 42. Winter, G. (2010). xia2: an expert system for macromolecular crystallography data reduction. *J. Appl. Crystallogr.* **43**, 186–190.
 43. Chen, V., Arendall, W. R., Headd, J., Keedy, D., Immormino, R., Kapral, G. *et al.* (2010). MolProbity: all-atom structure validation for macromolecular crystallography. *Acta Crystallogr., Sect. D: Biol. Crystallogr.* **66**, 12–21.
 44. Vagin, A. & Teplyakov, A. (1997). MOLREP: an Automated Program for Molecular Replacement. *J. Appl. Crystallogr.* **30**, 1022–1025.
 45. Emsley, P. & Cowtan, K. (2004). Coot: model-building tools for molecular graphics. *Acta Crystallogr., Sect. D: Biol. Crystallogr.* **60**, 2126–2132.
 46. Adams, P., Afonine, P., Bunkóczi, G., Chen, V., Davis, I., Echols, N. *et al.* (2010). PHENIX: a comprehensive Python-based system for macromolecular structure solution. *Acta Crystallogr., Sect. D: Biol. Crystallogr.* **66**, 213–221.
 47. Scott, J. & Smith, G. (1990). Searching for peptide ligands with an epitope library. *Science*, **249**, 386–390.
 48. Cwirla, S., Peters, E., Barrett, R. & Dower, W. (1990). Peptides on phage: a vast library of peptides for identifying ligands. *Proc. Natl. Acad. Sci. USA*, **87**, 6378–6382.